UNIVERSITY OF
ARKANSAS

SSRL

SSRL Report N° 2015-1

On the Fatigue Capacity of Headed Shear Studs in Composite Bridge Girders

Brianna Ovuoba
Gary S. Prinz, Ph.D., P.E.

November, 2015
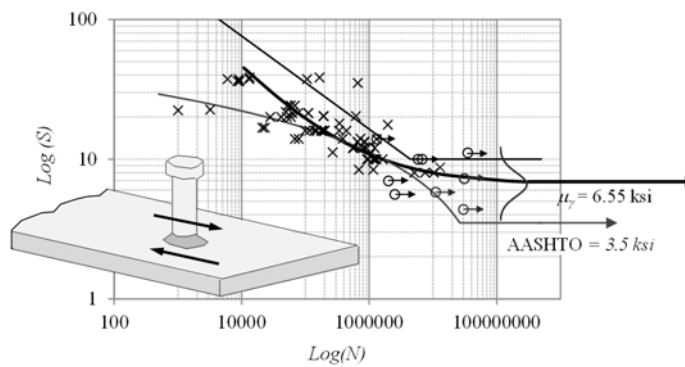
COLLEGE OF ENGINEERING
DEPARTMENT OF CIVIL ENGINEERING (CVEG)
STEEL STRUCTURES RESEARCH LABORATORY (SSRL)

University of Arkansas	Telephone :	+ 1 (479) 575-2494
Department of Civil Engineering	Fax :	+ 1 (479) 575-7168
4190 Bell Engineering Center	E-mail :	prinz@uark.edu
Fayetteville, AR 72701	Website :	www.ssrl-uark.com

UNIVERSITY OF
ARKANSAS

On the Fatigue Capacity of Headed Shear Studs in Composite Bridge Girders

Mandate: W&W | AFCO Steel

Mandate Description: Experimental and analytical investigation into the fatigue capacity of headed shear studs, with a focus on evaluating the location of the CAFL.

Date of Mandate: December, 2015

Specimens: 6 composite push-out specimens were tested.

Reception of the Specimens: December, 2014

Testing Dates: January 2015 – November 2015

Project PI: G.S. Prinz

Collaborators: B. Ovuoba, C. Dang, W.M. Hale

Report Authors: B. Ovuoba and G.S. Prinz

SSRL Director: G.S. Prinz

Signatures :
          Project PI

          Gary S. Prinz, PhD, PE

This report contains 41 pages (13 pages of front matter)

ACKNOWLEDGEMENTS

TABLE OF CONTENTS

LIST OF FIGURES

Appendix Figures:

LIST OF TABLES

Appendix Tables:

NOTATION

The following terms are used in the text of this report:

$(\Delta F)_n$	=	design load-induced fatigue resistance;
$(\Delta F)_{TH}$	=	the constant amplitude fatigue limit;
A	=	constant representing the intercept of the fatigue S-N curve;
$ADTT_{SL}$	=	single-lane average daily truck traffic (trucks);
BM	=	base metal;
$CAFL$	=	constant amplitude fatigue limit;
$CDF_{Ni,Si|\gamma'}$	=	cumulative density function assuming γ';
d	=	diameter of shear stud;
f'_c	=	concrete compressive strength;
f_{Ni}	=	probability of predicting failure at an individual data point;
$f_{Ni|\gamma'}$	=	probability of having failure at each given data point;
FZ	=	weld fusion zone;
$f_{\gamma'}$	=	probability that γ' exists;
HAZ	=	weld heat affected zone;
I	=	moment of inertia of the short-term composite section;
L	=	joint probability or likelihood;
$LVDT$	=	linear variable differential transducers;
m	=	constant representing the slope of the fatigue S-N curve;
MLE	=	maximum likelihood estimation;
N	=	number of cycles;
n	=	number of shear studs across the flange width;
n	=	required number of studs for the strength limit state;
N_f	=	number of cycles to failure;
n_f	=	total number of failure points;
n_r	=	total number of run-out points;
p	=	pitch (or spacing) of the row of shear studs along the length of the steel beam;
P	=	total nominal shear force;
$PDF_{Ni,Si|\gamma'}$	=	probability density function of failure at each given point;
$PDF_{Ni,\theta i}$	=	probability density function at fatigue test data point (N_i, θ_i);
PDF_{Ni}	=	marginal probability density function;
Q	=	first moment of the transformed short-term area of the concrete deck about the neutral axis of the short-term composite section;
Q_r	=	factored shear resistance of one shear connector;
R_{Ni}	=	probability of run-out;
$R_{Ni|\gamma'}$	=	probability of predicting run-out;
S	=	applied stress range;
V_f	=	vertical shear force range under the applicable fatigue loads;
V_{sr}	=	applied shear demand at the steel-concrete interface;
z^*	=	number of standard deviations shifted from the mean;
Z_r	=	fatigue shear resistance of an individual shear stud;
α	=	maximum likelihood fatigue-life curve parameter (power law constant);
β	=	maximum likelihood fatigue-life curve parameter (power law constant);
$\Delta\sigma$	=	applied stress range;
γ'	=	assumed constant amplitude fatigue limit;

REPORT SUMMARY

Shear connectors are commonly used in steel bridges to join the concrete deck and steel superstructure, providing a mechanism for shear transfer across the steel-concrete interface. The most common type of shear connector is the headed shear stud. In the current AASHTO LRFD bridge specifications on composite design, shear stud fatigue often governs over static strength, and a large number of shear connectors often result. The stud fatigue capacities presented in the AASHTO standard are largely based on a limited sample of composite fatigue tests performed in the 1960s, with limited fatigue test data at lower stress ranges leading to a somewhat arbitrary constant amplitude fatigue limit (CAFL). The somewhat arbitrary CAFL often governs the composite design for bridges with moderate-to-high traffic demands.

This report presents results from an experimental and analytical study into the fatigue behavior of headed shear studs, to address the lack of existing experimental data near the assumed CAFL, and to better characterize the effects of fatigue uncertainty on predicted response. Results from composite push-out specimens tested at low stress ranges between 30 and 60 MPa suggest a fatigue limit of 44.8MPa (6.5ksi) which is near the existing limit of 48 MPa (7ksi). Recommendations for modification to the existing AASHTO shear stud finite life S-N fatigue capacity curve are proposed.

FATIGUE TESTING REPORT

1. Introduction

1.1. *Background*

Shear connectors are commonly used in steel bridges to join the concrete deck and steel superstructure, providing a mechanism for shear transfer across the steel-concrete interface. Joining the steel and concrete members is advantageous, as the composite steel-concrete section has added strength over the sum of its individual components (the steel girder and concrete deck). This allows for use of lighter steel members and improved economy. The most common type of shear connector is the headed shear stud (see Figure 1(a)).

In the current AASHTO LRFD bridge specifications on composite design, shear studs must satisfy both strength and fatigue requirements [1]. To satisfy strength requirements, the shear connection between the concrete and steel elements must be capable of developing the full plastic capacity of the steel cross-section (create full composite action). To satisfy fatigue requirements, demands at the steel-concrete interface must be lower than the shear stud fatigue capacity as determined from an empirical fatigue capacity curve (called an S-N curve) and anticipated traffic cycles. Fatigue often governs, and a large number of shear connectors often result (see Figure 1(b)). Because traffic cycles are typically fixed from average daily truck traffic extrapolated over a 75-year design life, the S-N curve ultimately determines the required number of shear studs when the design is governed by fatigue.
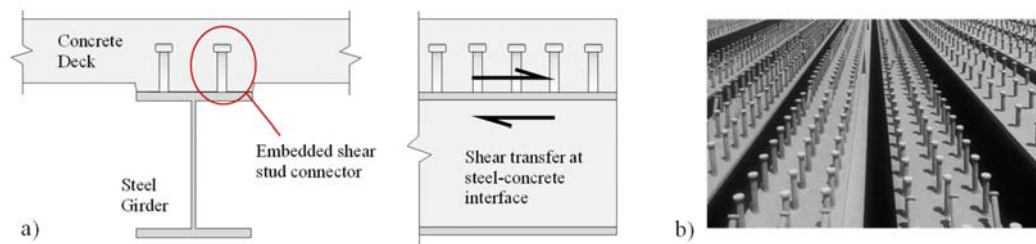
Figure 1. (a) Shear stud mechanism for load transfer across the steel-concrete interface, and (b) shop installed shear studs on a plate girder (photo courtesy of Bill McEleney, NSBA)

While many studies have investigated shear stud fatigue [2,3], the stud fatigue requirements in the AASHTO standard are largely based on single-sided push-out tests on 19mm (3/4 in) studs performed by Slutter and Fisher [4]. In the study by Slutter and Fisher, 26 samples containing 19mm (3/4in.) diameter studs were fatigue tested under constant amplitude stress cycles ranging in value from 55MPa (8ksi) to 138MPa (20ksi). To relate the applied stress range to the expected number of cycles for stud fatigue failure (S-N curve equations), a least-squares regression approach was used. Equation 1 presents the stud capacity equation based on the 26 data points from Slutter and Fisher [4], which shows similarity with the current stud fatigue capacity presented in the AASHTO standard [1] (see Equation 2). Note that the least-squares approach for regression analysis fails to account for any uncertainty distribution in the fatigue response, and therefore prevents the creation of characteristic capacity curves having known confidence levels.

$$\log(N) = 8.072 - 0.1753\,\Delta\sigma \qquad \text{(Eq. 1)} \;\; \text{Slutter and Fisher [4]}$$

$$\log(N) = 8.061 - 0.1834\,\Delta\sigma \qquad \text{(Eq. 2)} \;\; \text{AASHTO [1]}$$

The current AASHTO fatigue requirements assume a lower shear stud fatigue capacity than comparable specifications throughout the world. Figure 2 shows the current AASHTO shear stud design S-N curve along with a comparable curve from the European (Eurocode) standard [5]. Other shear stud S-N curves from the Japanese and British standards are similar in form to the Eurocode curve [6]. The AASHTO specification results in a lower estimation of stud fatigue capacity for all traffic demands, and considers a linear-log regression while the Eurocode, Japanese, and British standards consider log-log fatigue behavior. Note that the 24MPa (3.5ksi) fatigue limit shown in Figure 2 represents an effective "design" fatigue limit considering effects from variable amplitude loading (with the Fatigue I load factor of 2 incorporated [1]). This indicates a constant amplitude fatigue limit (CAFL) of 48MPa (7ksi) [1].

Limited fatigue test data exist at lower stress ranges to justify this CAFL location, which often governs the stud fatigue design for bridges with moderate-to-high traffic demands (ADTT greater than approximately 960 vehicles). Comparing the required number of studs in a rural short span steel bridge design (having a span of 17.3m (57ft)) at various levels of truck traffic, Lee et al. [6] found that bridges designed to the US requirements needed nearly twice as many shear studs than the corresponding European, British, and Japanese designs. In [6], stud capacities for the US designs were always governed by fatigue requirements.
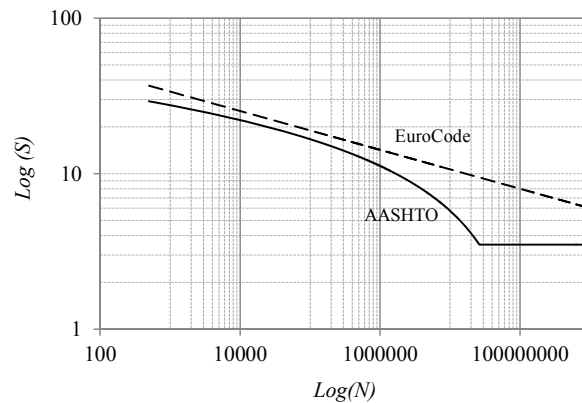
Figure 2. Comparison of design S-N curves for shear stud fatigue capacity between the AASHTO and Eurocode standards

This report presents an experimental and numerical study into the behavior of headed shear studs, to address the lack of existing experimental data near the assumed CAFL, and to better characterize the effects of fatigue uncertainty on predicted response. In this study, composite push-out specimens are fatigue tested at stress ranges near the existing AASHTO CAFL and a probabilistic approach is applied to both new and existing fatigue data to capture uncertainty and variation in the fatigue response.

1.2. *Report Overview*

The report begins by describing the experimental study, including the specimen geometry, test setup, instrumentation, and loading. Following, the experimental fatigue results are presented and a probabilistic method for fatigue data evaluation is described. Findings from the experimental study are combined with existing data from previous studies to provide a comprehensive data set for re-evaluation of shear stud fatigue capacity. A characteristic S-N curve for estimating shear stud fatigue capacity is proposed and applied to five prototype bridge designs to provide comparison.

2. Experimental Program

The primary objectives of the experimental program are to 1) characterize stud fatigue capacity at low applied stress ranges, 2) re-evaluate the existing CAFL considering both run-out and failure test results, and 3) investigate stud crack formation during low-stress high-cycle fatigue loading.

2.1. *Test Specimen Geometry and Fabrication*

Figure 3 shows the experimental push-out specimen geometry, consisting of a rolled W10x54 wide-flange section having 4 headed shear studs and a 6 in. cast-in-place concrete slab on each flange. The chosen geometry for the specimens (called herein double-sided push-out specimens) is based on guidelines for shear-stud testing prescribed in the Eurocode [7]. Double-sided push-out specimens are advantageous over single-sided push-out specimens (having a slab on only one side) as they help reduce loading eccentricities and multi-axial stress states within the stud (combined tension and shear). An applied multi-axial stress state in the stud can provide an overly-conservative estimation of fatigue capacity [3,6,8]. In this study, a total of 6 double-sided push-out fatigue tests are performed at four different applied stress levels ranging in value from 30MPa to 60MPa. Due to the significant time associated with high-cycle fatigue testing, only two replicate stress-ranges are considered in the test matrix (replicates at 40MPa and 60MPa).
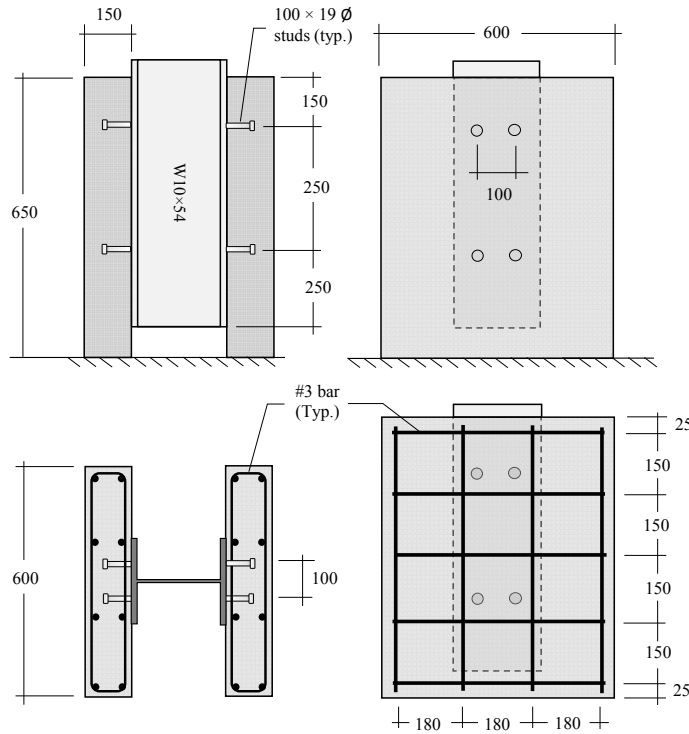
Figure 3. Push-out specimen geometry and slab rebar locations (all dimensions provided in mm) [7].

Concrete slabs of the test specimen are designed to represent typical composite bridge conditions. All concrete sections consider normal weight concrete from a standard highway bridge deck mix design [9], and each concrete section is cast with the beam in a horizontal position (see Figure 4). To ensure material consistency across the four different stress levels tested, four push-out specimens are simultaneously cast from the same concrete batch. Prior to each fatigue test, adequate concrete compressive strength (at least 80% f'_c) is checked from concrete cylinders formed during casting. Concrete strength data for each specimen are presented in Appendix B. To prevent adhesion between the concrete and steel, which can contribute to load transfer across the steel-concrete interface, each steel flange was coated in grease prior to concrete casting [7].

Figure 4. Casting of concrete slabs on double sided push-out specimens

2.2. *Test Configuration, Instrumentation, and Loading*

The experimental setup, shown in Figure 5(a), is designed to apply rapid shear stress cycles to studs within the push-out specimens. As shown in Figure 5(a), the double-sided push-out specimens are loaded with the beam oriented vertically, and the axial loads applied to the end of the steel wide-flange section. All specimens are subjected to unidirectional loading (specimens are loaded in one direction and then unloaded), resulting in a non-zero mean stress and providing a conservative fatigue loading condition as compared to reversed cycle loading [4]. To prevent separation between the specimen and testing machine at unloading, a pre-load of 1kN is maintained (somewhat shifting the applied mean stress). To ensure uniform contact between the concrete slabs and testing machine base, each specimen was leveled using a gypsum grout mixture.

Linear variable differential transducers (LVDTs) and unidirectional strain gauges are used to provide local measurements during testing. A total of eight LVDTs oriented parallel and perpendicular to the beam axis are included on each test specimen, to measure relative slip and separation between the concrete and steel sections. Unidirectional strain gauges are applied on two specimens to measure shear stresses transferred through the studs. Figure 5(b) shows the specimen instrumentation, including LVDT placement and strain gauge configurations.

Table 1 presents the experimental test matrix, including the specimen concrete strength, applied stress range, loading rate, and the resulting fatigue capacity. In Table 1, the applied stress ranges vary between 30MPa and 60MPa with specimen loading rates applied at between 10Hz and 20Hz. These high frequency loading rates are possible due to the high stiffness of the loading frame and test specimens. Note that measurements from several pseudo-static loading cycles applied at 1 Hz were used to verify negligible inertial effects at the higher frequency loading (see Appendix C for this verification). Fatigue results provided in Table 1 will be discussed in the following Results section.
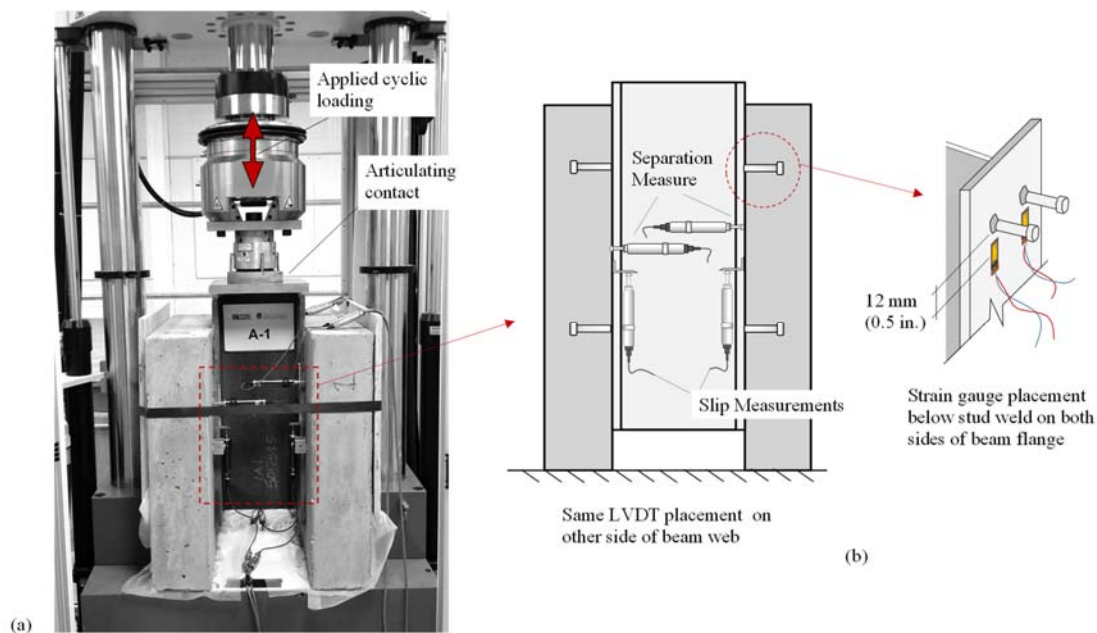
Figure 5. (a) Experimental setup and (b) specimen instrumentation

Table 1. Specimen Testing Matrix and Fatigue Results

Specimen Number	Average Concrete Compressive Strength [MPa]	Applied Stress Range [MPa]	Loading Rate [Hz]	Number of Cycles	Failure (F) or Runout (R)
1	40.87	60	10-20	12,803,000	F
2	48.15	30	10-20	30,053,000	R
3	44.16	40	10-20	12,251,908	R
4	56.37	40	10-20	20,000,000	R
5	44.40	50	10-20	31,401,000	R
6	57.61	60	10-20	30,001,000	R

3. Experimental Results

3.1. *Observations and Measured Fatigue Life*

All fatigue failures occurred at stress ranges above the existing AASHTO CAFL of 48.3MPa (7ksi), with the only complete fatigue failures occurring in Specimen 1 having an applied stress range of 60MPa. Failure in Specimen 1, evidenced by a complete fracture of the four embedded studs, occurred after 12.8 million cycles. In Specimen 1, fractures originated at the base of the stud weld (see Figure 6(c)) and propagated into the beam flange leaving crater-like indentations in the flange as shown in Figure 6(a). This failure mode is similar those observed in other push-out tests [4,10,11] and resulted in little-to-no damage to the concrete surrounding the stud. Specimen 2 (loaded at a stress range of 30 MPa) and Specimen 5 (loaded at a stress range of 50 MPa) survived more than 30 million cycles prior to being declared runouts. Specimens 3 and 4 loaded at 40 MPa were also declared runouts after 12.25 million and 20 million cycles respectively. The resulting fatigue capacities for all eight double-sided push-out specimens are provided in Table 1.

Slip between the concrete slab and steel beam was observed for all test specimens; however, for specimens loaded at stress ranges at or below 50MPa this slip was minor over then entire cycle history. Figure 7 shows the average slip for each slab of specimens 5 and 1 (loaded at 50MPa and 60MPa respectively). Slip measurements for other specimens having lower applied stress ranges were similar to Specimen 5, and are presented in the Appendix. The slip values presented in Figure 7 are computed by averaging the two LVDTs on each beam flange, providing a single slip value for each slab. In Figure 7 a noticeable slip in slab 1 of Specimen 1 occurs near 3 million cycles, followed by an increase in the slip-per-cycle rate up to failure of the studs at 12.8 million cycles. Slip between the concrete slab and steel beam is an indication of stiffness loss and possible stud damage. Specimen 5, subjected to a lower applied stress range, experienced minimal slip (suggesting little stud damage) over the entire 30 million cycle loading. While slip measurements are helpful in estimating damage within the embedded studs over time, more detailed investigations are required to determine whether fatigue cracks actually exist.

a) Steel Flange Surface   b) Concrete Surface   c) Removed Shear Stud
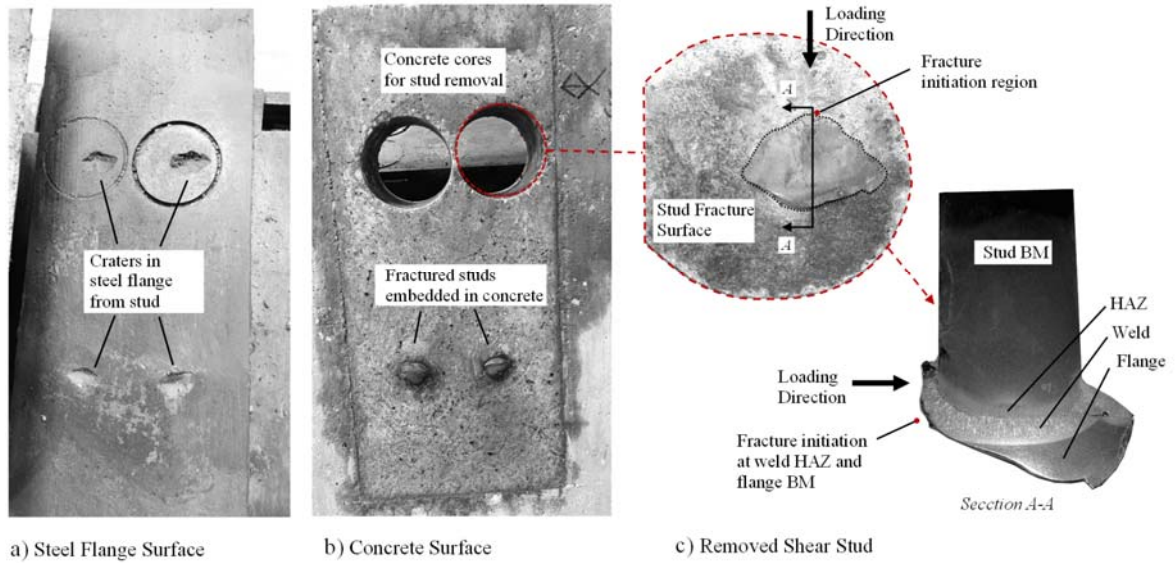
Figure 6. Shear stud failure mode observations for Specimen 1 (failure observed after 12,803,000 cycles at an applied stress range per stud of 60MPa)
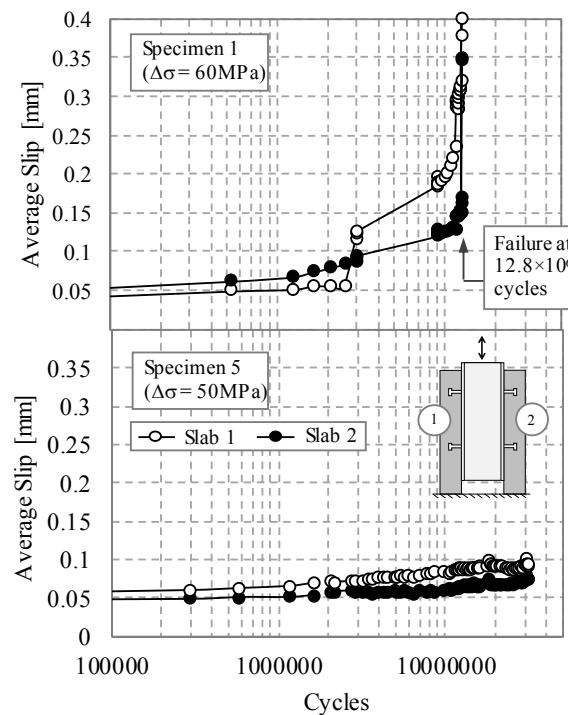
Figure 7. Average slip versus number of applied cycles for Specimens 1 and 5.

3.2. *Stud Fatigue-Crack Investigations*

Metallographic investigation and micro-hardness testing of stud cross-sections cored from completed tests indicate fatigue crack initiations within runout specimens and a critical

fracture location near the stud-to-flange weld heat affected zone (HAZ). Stud samples cored from runout Specimens 2 and 5, were sectioned, polished with abrasive paper and diamond powder of increasing fineness (mirror polished to a surface roughness of 1μm), and then surface etched with a Nitol solution (5ml HNO3 per 100ml of ethanol). Figure 8 shows the polished stud cross-sections taken from the specimens with the various weld features highlighted, including the weld HAZ, base metals (BM), and fusion zone (FZ). Vickers micro-hardness measurements (shown as contours in Figure 8) highlight material property changes (potential changes in material toughness) within the welded stud-to-flange zone and confirm the location of the HAZ, FZ, and BM. Stud sections taken from Specimen 2 (declared a runout after more than 30 million cycles at 30MPa) show no indication of fatigue crack initiation (see Figure 8(a)); however, samples taken from Specimen 5 (declared a runout after more than 30 million cycles at 50MPa) indicate fatigue cracks initiating near the weld HAZ at the stud-to-flange interface (see Figure 8(b)). The initiated fracture observed in Specimen 5 closely resembles the fracture path shown in Figure 6(c) for failure Specimen 1. These initiated fatigue cracks were present in all studs cored from Specimen 5.
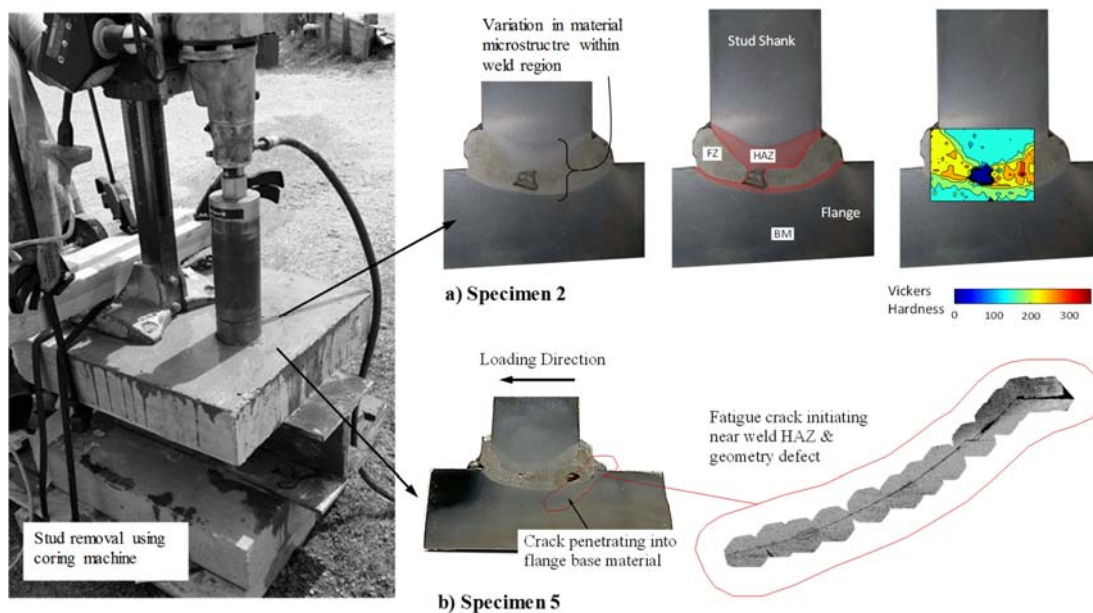
Figure 8. Fatigue crack investigation of polished stud sections from (a) Specimen 2 and (b) Specimen 5

4. Probabilistic Approach to Shear Stud Fatigue Capacity Evaluation

Scatter in fatigue test results is inevitable, and can provide uncertainty when predicting fatigue performance. When creating S-N curves for fatigue prediction, quantifying this uncertainty and maximizing the likelihood of predicting an experimental outcome is desired. In the regression analysis by Slutter and Fisher [4] (on which the current AASHTO stud capacity limits are based), S-N curves for shear stud fatigue capacity were created using a simplified least-squares fitting procedure incapable of quantifying the uncertainty in the experimental scatter. In this section, an alternative curve creation approach is proposed, wherein an advanced statistical method called maximum likelihood estimation (MLE) is used to create S-N curves that maximize the joint probability of predicting the observed experimental result. Several studies have successfully used MLE to define curve regressions for large data sets [12,13,14,15]. The following paragraphs describe a random fatigue limit model proposed by

Pascual et al. [16] using the MLE method. The newly generated shear stud fatigue data is combined with existing data from the previous studies and analyzed using the random fatigue limit model. A new characteristic shear stud S-N curve considering data uncertainty and having a known confidence level is proposed.

4.1. *Overview of MLE*

The goal of the MLE approach is to identify a population (probability distribution) at each stress level that is most likely to have generated the experimental data. To achieve this, parameters for the population are chosen that maximize the joint probability of predicting failure at all points (or in other words, to maximize the likelihood of predicting failure at all points). This joint failure probability (or likelihood) is simply the product of every data-point failure probability, written as:

$$L = \prod_{i=1}^{nf} f_{N_i} \cdot \prod_{i=1}^{nr} R_{N_i}$$

(Eq. 3)

where, L, f_{Ni}, R_{Ni}, n_f and n_r are the likelihood, probability of predicting failure at an individual data point (i), the probability of predicting run-out at an individual data point (i), the total number of failure data-points, and the total number of run-out points respectively.

In this study, a nonlinear generalized reduced gradient optimization algorithm is used to maximize the likelihood given by the variable parameters in the regression model. In determining the individual failure probabilities required in Equation 3, a power-law relationship is assumed to appropriately represent the fatigue data [17,18]. This power-law relationship is given in Equation 4,

$$\log_e N = \alpha + \beta \log_e (S - \gamma')$$

(Eq. 4)

where N is the number of cycles to failure at a given applied stress range, S. Parameters α and β in Equation 4 are unknown parameters to be determined through MLE and γ' is the assumed CAFL, also to be determined through MLE. Note that for a confidence level of 50%, γ' in Equation 4 will be equal to the mean, μ_γ, of the CAFL distribution. For other curve confidence levels, γ' is taken as μ_γ- $z^*\sigma_\gamma$ (shifting the CAFL location z* standard deviations from the mean). Equation 5 presents the regression relationship that can be used for confidence levels other than the mean, and Figure 9 depicts the MLE based model assuming the above power-law relationship and considering normally distributed data at each stress-range level.

$$\log_e N = \alpha + \beta \log_e (S - (\mu_\gamma - z^* \sigma_\gamma)) - z^* \sigma$$

(Eq. 5)
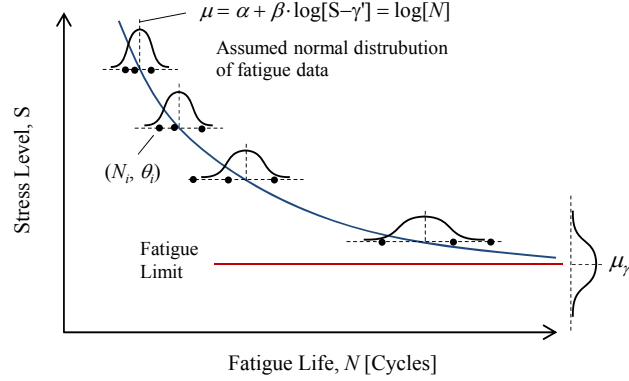
Figure 9. Fatigue-life curve representation through MLE fitting

The probability of having failure at each data point (N_i, S_i) in Figure 9, given a specific CAFL value (γ') and assuming the data at each stress-range level as normally distributed, is given by the conditional probability density function shown in Equation 6.

$$f_{N_i|\gamma'} = PDF_{N_i,S_i|\gamma'} = \left(\frac{1}{\sqrt{2\pi}\cdot\sigma}\right)\exp\left(\frac{-1}{2\sigma^2}\cdot[N_i - \alpha - \beta\log(S_i - \gamma')]^2\right) \qquad \text{(Eq. 6)}$$

Because $f_{N_i|\gamma'}$ assumes a given γ', the probability that γ' exists $(f_{\gamma'})$ must also be determined (see Equation 7). The resulting probability of predicting failure at N_i is the marginal probability density function representing the joint probability between $f_{N_i|\gamma'}$ and $f_{\gamma'}$ as given in Equation 8.

$$f_{\gamma'} = \left(\frac{1}{\sqrt{2\pi}\cdot\sigma_{\gamma'}}\right)\exp\left(\frac{-1}{2\sigma_{\gamma'}^2}\cdot[\gamma'-\mu_\gamma]^2\right) \qquad \text{(Eq. 7)}$$

$$f_{Ni} = PDF_{N_i} = \int_0^{S_i} f_{N_i|\gamma'}\cdot f_{\gamma'}\cdot d\gamma' \qquad \text{(Eq. 8)}$$

4.2. Influence of Run-Outs on CAFL

Many S-N curves often only consider failure test results in identifying regression parameters, neglecting run-out test results and their potential influence on curve features such as the CAFL. At certain low stress levels, such as those considered in this study, the possibility exists for run-out test results to occur. MLE allows these run-out test results to influence the S-N curve through the population cumulative distribution function, since run-out simply indicates the absence of failure. In the case of run-outs, the probability of predicting run-out given an assumed CAFL (γ') is given by:

$$R_{N_i|\gamma'} = 1 - CDF_{N_i,S_i|\gamma'} \qquad \text{(Eq. 9)}$$

where $CDF_{Ni,Si|\gamma'}$ is the cumulative density function assuming γ'. The resulting probability of run-out, R_{Ni}, is the marginal probability density function between Equation 9 and Equation 7, given by equation 10.

$$R_{N_i} = \int_0^{S_i} (1 - CDF_{N_i, S_i | \gamma'}) \cdot f_{\gamma'} d\gamma' \qquad\qquad\qquad \text{(Eq. 10)}$$

4.3. *Shear Stud Fatigue Dataset and Analysis using MLE*

The complete fatigue data set considered in this study is presented in Table A- 1 of Appendix A, and consists of the six fatigue results described earlier and 100 fatigue results from existing comparable testing found in the literature. The 100 fatigue results taken from the literature were from a total of seven shear stud fatigue studies conducted between 1959 and 1988 [4,10,19,20,21,22,23]. All existing fatigue data presented in Table A- 1 were selected based on four criteria, including: 1) a stud shank diameter of 19mm (3/4 in.); 2) constant amplitude loading; 3) unidirectional loading (no reversed cycles), and 4) failure occurring in the stud shank or weld (i.e. no concrete crushing failures). For conservancy, test results from reversed cycle loading were not included, as they typically result in higher fatigue capacities due to the reduced applied mean stress [4]. Fatigue results from both single-sided and double-sided push-out tests were considered. Additional test data for 7/8" studs from more recent studies (conducted between 2000 and 2014) are used in comparisons (see Table A- 2) [4,8,11,24,25,26].

Analysis of the fatigue dataset suggests that the existing AASHTO CAFL is reasonable, but indicates higher fatigue capacity within the finite-life region for stress-ranges over 117MPa (17ksi). Equation 11 presents the stud fatigue capacity equation resulting from the MLE analysis, with the optimized parameters of α, β, μ_γ, σ, and σ_γ being 17.26, -2.09, 6.5ksi, 1.45, and 1.21ksi respectively. Note that the stress range parameter in Equation 11 is based on units of ksi. The resulting distribution for the CAFL is characterized by a standard deviation of 1.21ksi. In Equation 11, the mean CAFL value of 44.8MPa (6.5ksi) is near the existing value of 48MPa (7ksi) for constant amplitude fatigue. Analysis of the data considered uniformly distributed data at each stress-range level, and a mean confidence level (50%) based on the inherent conservancies in fatigue data resulting from push-out specimens [4,6,26].

$$\log_e N = 17.26 - 2.09 \log_e (S - 6.5) \qquad\qquad\qquad \text{(Eq. 11)}$$

Figure 10 shows the resulting regression from the MLE analysis. For comparison, the current AASHTO shear stud S-N curve is also plotted along with the considered fatigue data-set.
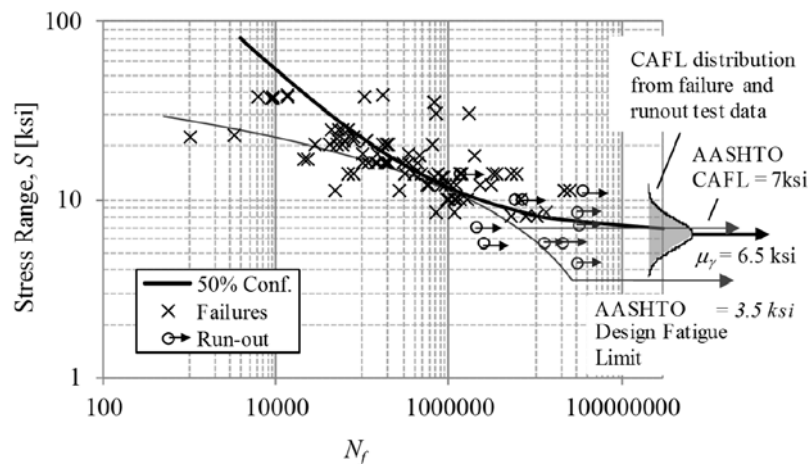
Figure 10. Comparison of AASHTO S-N curve and MLE regression

5. Proposed Design S-N Curve for Predicting Shear Stud Fatigue Capacity

Given similarities in form between the MLE S-N curve and the S-N curves for various steel bridge fatigue details provided in AASHTO, a simplification of Equation 11 is proposed to provide consistency in design. In AASHTO [1], the design load-induced fatigue resistance for bridge details (excepting fatigue of the stud) takes the form:

$$\left(\Delta F\right)_n = \left(\frac{A}{N}\right)^{\frac{1}{m}} \geq \left(\Delta F\right)_{TH}$$

(Eq. 12)

where m and A are constants representing the slope and intercept of the fatigue S-N curve. In Equation 12, $(\Delta F)_{TH}$ is the CAFL, and $(\Delta F)_n$ is the allowable stress range. To adapt Equation 11 to the form provided in Equation 12, a bi-linear design S-N curve is fit to the power-law relationship determined through MLE using the CAFL asymptote and approximate tangent at 103MPa (15ksi). This simplification provides an avenue for consistency between shear stud fatigue capacities and standard fatigue detail capacity forms. Table 2 presents the proposed detail category description, including the proposed S-N curve constant (A), slope (m), threshold value (CAFL or $(\Delta F)_{TH}$), description of the potential crack initiation point, and an illustrative example of potential damage.

Table 2: Proposed detail category description for shear stud fatigue capacity

Description	Category	Constant A (ksi⁴)	Threshold $(\Delta F)_{TH}$ ksi	Potential Crack Initiation Point	Illustrative Examples
9.2 Connection weld or shank of stud-type shear connector attached by fillet or automatic stud welding subjected to shear loading	D' [$m = 4$]	150×10^8	6.5	Toe of stud-to-flange welds, propagating through the stud shank or into the flange base metal	

Figure 11(a) plots the proposed design S-N curve along with the MLE regression and fatigue data, and Figure 11(b) compares the proposed bi-linear design S-N curve with the current AASHTO fatigue detail categories. Note in Figure 11(b), that the proposed stud fatigue design S-N curve indicates a lower fatigue capacity than the curve for fracture in the base metal outside the stud weld, but a higher capacity than the current AASHTO stud fatigue limit. While the proposed design S-N curve is derived from the MLE analysis on ¾" stud fatigue tests, data from other fatigue tests on ½", 7/8", and 1-1/4" studs fits the general trend of the curve and fall within the scatter of the ¾" results. For comparison, Figure 11(c) is provided to show the proposed design S-N curve with data from ¾", ½", 7/8", and 1-1/4" stud fatigue tests (see Appendix A for the stud fatigue values considered).
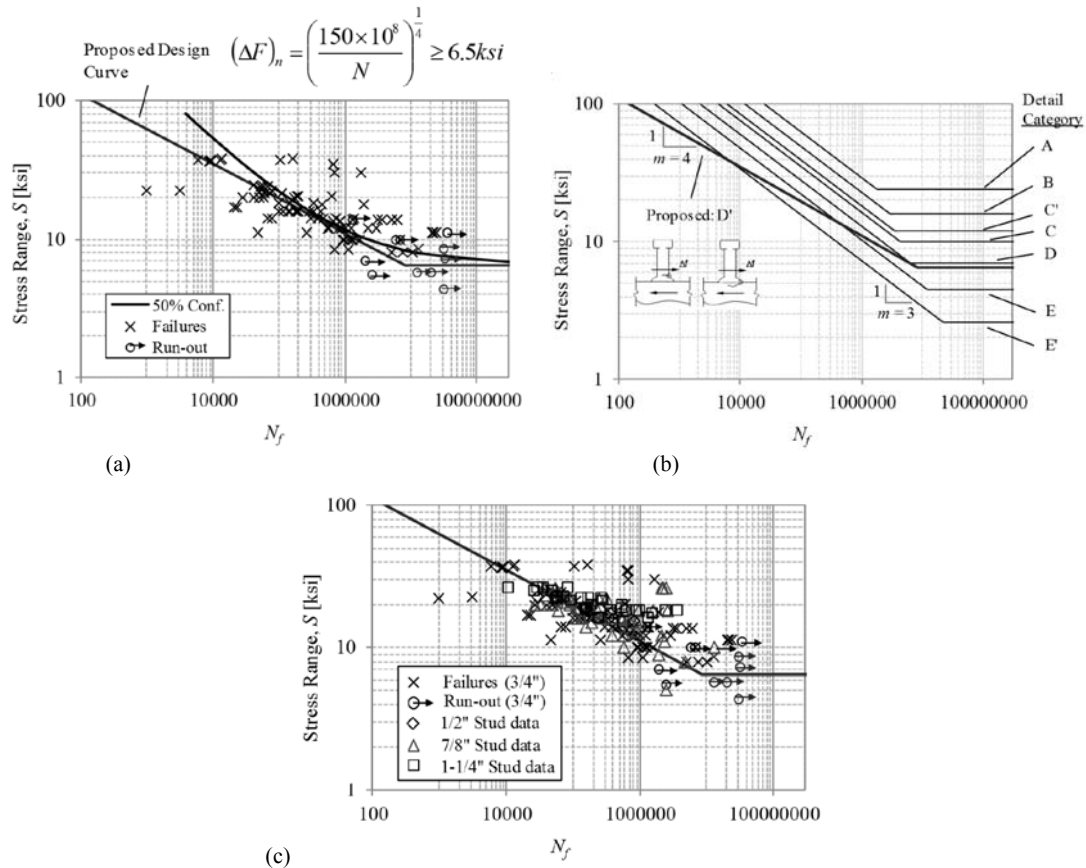
Figure 11. (a) Comparison of proposed design S-N curve, MLE regression, fatigue data, and current AASHTO curve; (b) Comparison of proposed design S-N curve and existing AASHTO fatigue details; (c) comparison of proposed curve with fatigue data from additional stud diameters other than ¾".

6. Summary and Conclusions

In this study, six composite push-out specimens were fatigue tested under repeated cyclic loads at stress ranges varying between 30MPa and 60MPa. These composite push-out specimens represent a conservative estimation of stud fatigue damage as the adhesion and friction at the steel-concrete interface were inhibited by greasing of the steel flanges prior to concrete casting. Measured fatigue life from the eight specimens were combined with existing shear stud fatigue data sets in the literature, and analyzed using a probabilistic method called maximum likelihood estimation. Results from the six fatigue tests and analysis of the new and existing fatigue data provide the following conclusions:

1) The current AASHTO CAFL for headed shear studs provides a reasonable estimation of fatigue capacity. Analysis of existing data along with the additional high-cycle fatigue test results suggests a CAFL of 44.8MPa (6.5ksi) which is near the assumed value of 48 MPa (7ksi).

2) The current AASHTO S-N curve for finite life of the shear stud underestimates fatigue capacity and is not representative of the larger considered fatigue dataset. An alternative design S-N curve of similar form to the existing AASHTO detail categories

(log-log form) is proposed. The proposed curve of the form $(\Delta F)_n = \left(\dfrac{A}{N}\right)^{\frac{1}{m}} \geq (\Delta F)_{TH}$ has an *m*=4 and *A*= 150x10^8 and provides a known level of confidence in the estimated fatigue capacity (based on the MLE analysis with a confidence level of 50%) while providing a unification in the fatigue design procedure. Note that stress range capacities provided in the proposed equation were derived using imperial units of ksi.

7. References

[1]   AASHTO (2012). "AASHTO LRFD bridge design specifications (6th edition)." *American Association of State Highway and Transportation Officials*, Washington, DC.

[2]   Oehlers, D. J. (1990). "Methods of estimating the fatigue enduraces of stud shear connections." *IABSE Proceedings P-145/90*, p. 65-84.

[3]   Johnson, R. P. (2000). "Resistance of stud shear connectors to fatigue." *J. Constructional Steel Research* 56(2000), 101-116.

[4]   Slutter, R. G., and Fisher, J.W. (1966). "Fatigue strength of shear connectors " *Highway Research Record No. 147*, Highway Research Board, p. 65-88.

[5]   Eurocode_4 (1994). "Design of composite steel and concrete structures - Part 2: General rules and rules for bridges." *ENV 1994-2*, European Committee for Standardization, Brussels, Belgium.

[6]   Lee, K.-C., Abbas, H.H., and Ramey, G.E. (2010). "Review of current AASHTO fatigue design specifications for stud shear connectors." *ASCE Structures Congress Proceedings*, p. 310-321.

[7]   Eurocode_4 (1994). "Design of composite steel and concrete structures - Part 1-1: General rules and rules for buildings." *ENV 1994-1-1*, European Committee for Standardization, Brussels, Belgium.

[8]   Badie, S. S., Tadros, M.K., Kakish, H.F., Splittgerber, D.L., and Baishya, M.C. (2002). "Large shear studs for composite action in steel bridges." *J. Bridge Engineering, ASCE* 7(3), p.195-203.

[9]   AHTD (2014). "Division 800, Section 802: Concrete for structures." *The Arkansas Standard Specification for Highway Construction*

[10]   Hallam, M. W. (1976). "The behaviour of stud shear connectors under repeated loading." *Research Report No, R281*, University of Sydney, School of Civil Engineering, Sydney, Austrailia.

[11]   Feldmann, M., Hechler, O., Hegger, J., and Rauscher, S. (2011). "Fatigue behavior of shear connectors in high performance concrete." *Composite Construction in Steel and Concrete VI*, pp. 39-51, doi: 10.1061/41142(41396)41144

[12]   D'Angelo, L., Rocha, M., Nussbaumer, A., and Bruhwiler, E. (2014). "Creation of S-N-P curves for reinforcing steel bars using a maximum likelihood approach." *Proc. Eurosteel*, Naples, Italy.

[13]   Myers, A. T., Kanvinde, A.M., and Ibarra, L. (2012). "Maximum likelihood based parameter estimation of constitutive models for earthquake engineering." *15th World Conference on Earthquake Engineering*, Lisbon, Portugal.

[14]   Prinz, G. S., and Nussbaumer, A. (2014). "Effect of radial base-plate welds on ULCF capacity of unanchored tank connections." *J. Constructional Steel Research* 103(2014), 131-139.

[15]   Ling, J., and Pan, J. (1997). "A maximum likelihood method for estimating P-S-N curves." *International J. of Fatigue* 19(5), 415-419.

[16]   Pascual, F. G., and Meeker, W.Q. (1999). "Estimating fatigue curves with the random fatigue-limit model: 1 Introduction." *Technometrics* 1999

[17]   Coffin, L. F. (1954). "A study of the effects of cyclic thermal stresses in ductile metals." *ASME,* 76, 931-950.

[18]   Manson, S. S. (1954). Behavior of materials under conditions of thermal stress. <u>National Advisory Committee for Aeronautics,</u>. Technical note 2933. Tennessee (USA).

[19]   Mainstone, R. J., and Menzies, J.B. (1967). "Shear connectors in steel-concrete composte beams for bridges, Part I." *Concrete* 1(9), pp. 291-302.

[20]   Lehman, H. G., Lew, H.S., and Toprac, A.A. (1965). "Fatigue strength of 3/4 inch studs in lightweight concrete." *Research Report No. 76-1F*, Center for Highway Research, The University of Texas, Austin, Texas.

[21]   Naithani, K. C., Gupta, V.K., and Gadh, A.D. (1988). "Behaviour of shear connectors under dynamic loads." *Materials and Structures* 21

[22]   Roderick, J. W., and Ansorian, P. (1976). "Repeated loading of composite beams." *Civil Engineering Transactions* CE18(2), pp. 109-116.

[23]   Thurlimann, B. (1959). "Fatigue and static strength of steel shear connectors, Lehigh University, 1959 Reprint No. 144(59-8)." (1959) Fritz Laboratory Reports. Paper 1253.

[24]   Mundie, D. L. (2011). "Fatigue testing and design of large diameter shear studs used in highway bridges." *Masters Thesis*, Auburn University, Auburn, AL.

[25]   Faust, T., Leffer, A., and Mesinger, M. (2000). "Fatigue of headed studs embedded in LWAC." *Second International Symposium on Structural Lightweight Aggregate Concrete* 2(2000), pp.212-220.

[26]   Provines, J., and Ocel, J.M. (2014). "Strength and fatigue resistance of shear stud connectors." *National Accelerated Bridge Construction Conference (ABC)*, December, 4-5, Miami, Florida.

[27]   ASTM (2008). Standard practice for making and curing concrete test specimens in the field. <u>C31/C31M-09</u>. West Conshohicken, Pa.

[28]   ASTM (2015). Standard test method for compressive strength of cyllidrical concrete specimens. <u>C39/C39M-15a</u>. West Conshohicken, Pa.

Appendix A. Shear Stud Fatigue Dataset

Table A- 1 provides the ¾" stud fatigue data set values used in determining the proposed design S-N curve. Table A- 2 provides the 7/8" stud fatigue values used in comparison. Failure modes described in Tables A-1 and A-2 refer to type A, B, or C fractures as shown in Figure A- 1.
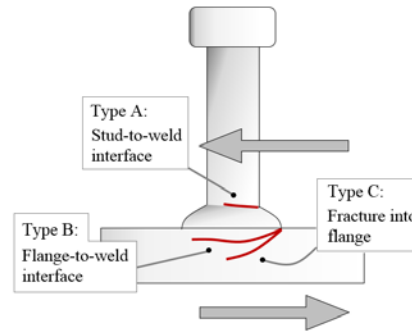
Figure A- 1. Common (type A, B, and C) fatigue
fractures within shear stud connectors.

Table A- 1. Fatigue dataset for ¾" diameter shear studs

Reference	Test Number	Specimen Name	No. of Slabs in Test	Studs/Side	Failure Mode	Stress Range (ksi)	N_f (cycles)
Hallam[1]	1	PS4	2	2	Type A	24.19	52,801
Hallam	2	PS42	2	2	Type A	24.19	52,836
Hallam	3	PS5	2	2	Type A	24.19	58,630
Hallam	4	PS52	2	2	Type A	24.19	67,877
Hallam	5	PS10	2	2	Type A	21.39	61,700
Hallam	6	PS102	2	2	Type A	21.39	75,500
Hallam	7	PS11	2	2	Type A	21.39	110,000
Hallam	8	PS112	2	2	Type A	21.39	110,000
Hallam	9	PS12	2	2	Type A	15.99	148,700
Hallam	10	PS122	2	2	Type A	15.99	174,800
Hallam	11	PS13	2	2	Type A	15.99	182,600
Hallam	12	PS132	2	2	Type A	15.99	182,600
Hallam	13	PS12	2	2	Run-Out	13.89	1,303,669
Hallam	14	PS1	2	2	Type A	13.89	1,303,669
Hallam	15	PS3	2	2	Type A	13.30	652,300
Hallam	16	PS32	2	2	Type A	13.30	652,300
Hallam	17	PS2	2	2	Type A	13.30	823,970
Hallam	18	PS22	2	2	Type A	13.30	845,000
Hallam	19	PS6	2	2	Type C	13.70	3,170,000
Hallam	20	PS62	2	2	Type C	13.70	3,554,000
Hallam	21	PS7	2	2	Type C	13.70	5,140,000
Hallam	22	PS72	2	2	Type C	13.70	6,096,000
Hallam	23	PS82	2	2	Type C	11.10	20,965,000
Hallam	24	PS8	2	2	Type C	11.10	21,391,000
Hallam	25	PS9	2	2	Type C	11.10	24,305,000

↓ Continued ↓

Table A-1: Continued…

Reference	Test Number	Specimen Name	No. of Slabs in Test	Studs/Side	Failure Mode	Stress Range (ksi)	N_f (cycles)
Hallam	26	PS92	2	2	Run-Out	11.10	35,000,000
Lehman/Lew[2]	1	212	2	4	Run-Out	10.00	6,730,000
Lehman/Lew	2	616	2	4	Run-Out	10.00	5,810,000
Lehman/Lew	3	1020	2	4	Type B/C	10.00	6,711,000
Lehman/Lew	4	214	2	4	Type B/C	12.00	2,960,000
Lehman/Lew	5	618	2	4	Type B/C	12.00	2,223,000
Lehman/Lew	6	216	2	4	Type B/C	14.00	305,000
Lehman/Lew	7	620	2	4	Type B/C	14.00	1,345,000
Lehman/Lew	8	1024	2	4	Type B/C	14.00	390,000
Lehman/Lew	9	620B	2	4	Type B/C	14.00	726,000
Lehman/Lew	10	218	2	4	Type B/C	16.00	292,000
Lehman/Lew	11	622	2	4	Type A	16.00	435,720
Lehman/Lew	12	220	2	4	Type B/C	18.00	100,000
Lehman/Lew	13	624	2	4	Type B/C	18.00	142,680
Lehman/Lew	14	1028	2	4	Type B/C	18.00	340,300
Mainstone[3]	1	S1	2	2	Type B/C	22.18	76,000
Mainstone	2	S10	2	2	Type B/C	28.07	1,700,000
Mainstone	3	S12	2	2	Type B/C	31.69	679,000
Mainstone	4	S2	2	2	Type B/C	17.66	439,000
Mainstone	5	S20	2	2	Type B/C	35.08	669,000
Mainstone	6	S23	2	2	Stud[9]	35.08	657,000
Mainstone	7	S24	2	2	Yield	36.22	9,200
Mainstone	8	S25	2	2	Stud	38.48	13,300
Mainstone	9	S27	2	2	Stud	37.35	8,970
Mainstone	10	S28	2	2	Stud	37.35	6,000
Mainstone	11	S30	2	2	Yield	37.35	13,100
Mainstone	12	S31	2	2	Stud	36.22	8,600
Mainstone	13	S32	2	2	Stud	38.48	165,000
Mainstone	14	S33	2	2	Stud	37.35	106,000
Mainstone	15	S7	2	2	Stud	17.66	1,940,000
Mainstone	16	S9	2	2	Type B/C	24.45	42,000
Nathani[4]	2	F2	1	1	Stud	22.64	3,200
Nathani	3	F1	1	1	Stud	22.36	1,000
Nathani	4	F3	1	1	Stud	16.77	23,000
Nathani	5	F4	1	1	Stud	16.77	21,000
Nathani	6	F5	1	1	Stud	13.98	68,000
Nathani	7	F6	1	1	Stud	13.98	78,000
Nathani	8	F7	1	1	Stud	11.18	266,000
Nathani	9	F8*	1	1	Type B/C	11.18	48,000
Nathani	10	F10	1	1	Stud	8.39	685,000
Nathani	11	F9+	1	1	Stud	8.39	1,150,000
Nathani	12	F11	1	1	Run-Out	6.99	2,000,000
Nathani	13	F12	1	1	Run-Out	5.59	2,512,000
Roderick[5]	1	R4	2	2	Yield	21.76	49,300
Roderick	2	R1	2	2	Yield	20.30	616,000
Roderick	3	R2	2	2	Yield	20.30	194,110
Roderick	4	R3	2	2	Yield	20.30	190,460
Slutter/Fisher[6]	1	a3C	1	4	Type B/C	8.00	7,481,100
Slutter/Fisher	2	b3C	1	4	Type B/C	8.00	10,275,900
Slutter/Fisher	3	c3C	1	4	Type B/C	8.00	5,091,200
Slutter/Fisher	4	a6B	1	4	Type B/C	10.00	962,500
Slutter/Fisher	5	b6B	1	4	Type B/C	10.00	919,100

↓ Continued ↓

Table A-1. Continued…

Reference	Test Number	Specimen Name	No. of Slabs in Test	Studs/Side	Failure Mode	Stress Range (ksi)	N_f (cycles)
Slutter/Fisher	6	c6B	1	4	Type B/C	10.00	1,144,600
Slutter/Fisher	7	a6C	1	4	Type B/C	10.00	1,213,600
Slutter/Fisher	8	b6C	1	4	Type B/C	10.00	1,295,300
Slutter/Fisher	9	c6C	1	4	Type B/C	10.00	1,618,900
Slutter/Fisher	10	a2B	1	4	Type B/C	12.00	897,300
Slutter/Fisher	11	b2B	1	4	Type B/C	12.00	565,300
Slutter/Fisher	12	c2B	1	4	Type B/C	12.00	551,100
Slutter/Fisher	13	a4C	1	4	Type B/C	12.00	798,000
Slutter/Fisher	14	b4C	1	4	Type B/C	12.00	1,215,400
Slutter/Fisher	15	c4C	1	4	Type B/C	12.00	1,010,400
Slutter/Fisher	16	P2	1	4	Type B/C	14.00	383,600
Slutter/Fisher	17	a3B	1	4	Type B/C	16.00	139,400
Slutter/Fisher	18	b3B	1	4	Type B/C	16.00	114,700
Slutter/Fisher	19	c3B	1	4	Type B/C	16.00	199,500
Slutter/Fisher	20	a5C	1	4	Type B/C	16.00	335,800
Slutter/Fisher	21	b5C	1	4	Type B/C	16.00	99,200
Slutter/Fisher	22	c5C	1	4	Type B/C	16.00	197,000
Slutter/Fisher	23	P1	1	4	Type B/C	20.00	27,900
Slutter/Fisher	24	a4B	1	4	Type B/C	20.00	41,500
Slutter/Fisher	25	b4B	1	4	Type B/C	20.00	50,700
Slutter/Fisher	26	c4B	1	4	Type B/C	20.00	58,700
Thurlimann[7]	1	9	2	4	N.S.[10]	20.00	169,000
Thurlimann	2	10	2	4	N.S.	14	474,000
Ovuoba/Prinz[8]	1	1	2	4	Type C	8.70	12,803,000
Ovuoba/Prinz	2	2	2	4	Run-Out	4.4	30,053,000
Ovuoba/Prinz	3	3	2	4	Run-Out	5.8	12,251,908
Ovuoba/Prinz	4	4	2	4	Run-Out	5.8	20,000,000
Ovuoba/Prinz	5	5	2	4	Run-Out	7.3	31,401,000
Ovuoba/Prinz	6	6	2	4	Run-Out	8.7	30,001,000

[1] Hallam, M.W. (1976) [10]

[2] Lehman, H.G., Lew, H.S., and Toprac, A.A. (1965) [20]

[3] Mainstone, R.J., and Menzies, J.B. (1967) [19]

[4] Nathini, K.C., Gupta, V.K., and Gadh, A.D. (1988) [21]

[5] Roderick, J.W., and Ansorian, P. (1976) [22]

[6] Slutter, R.G., and Fisher, J.W. (1966) [4]

[7] Thurlimann, B. (1959) [23]

[8] Ovuoba and Prinz (Current test report)

[9] Failure occurred near mid height of stud shank

[10] Failure mode not specified

Table A- 2. Fatigue dataset for 7/8" diameter shear studs

Reference	Test Number	Specimen Name	No. of Slabs in Test	Studs/Side	Failure Mode	Stress Range (ksi)	N_f (cycles)
Feldman[1]	1	HSIt1	2	4	Type B/C	26.3	2113520
Feldman	2	HSIt2	2	4	Type B/C	26.3	2265273
Feldman	3	HSIt3	2	4	Type B/C	26.3	2505680
Slutter/Fisher	1	e3I	1	4		8	4885100
Slutter/Fisher	2	e2H	1	4		12	2133000
Slutter/Fisher	3	e4I	1	4		12	587700
Slutter/Fisher	4	e3H	1	4		16	112500
Slutter/Fisher	5	e5I	1	4		16	134300
Slutter/Fisher	6	e4H	1	4		20	33000
Badie/Tadros[2]	1	SS-5-25	1	8	Stud	20	27000
Badie/Tadros	2	SS-5-23	1	8	Stud	18	60000
Badie/Tadros	3	SS-5-21	1	8	Stud	16	285000
Badie/Tadros	4	SS-5-20	1	8	Stud	15	189000
Badie/Tadros	5	SS-5-19	1	8	Stud	14	157000
Badie/Tadros	6	SS-5-18	1	8	Stud	13	935000
Badie/Tadros	7	SS-5-17	1	8	Concrete	12	400000
Badie/Tadros	8	SS-5-16	1	8	Stud	11	2452000
Badie/Tadros	9	SS-5-15	1	8	Stud	10	600000
Badie/Tadros	10	SS-5-14	1	8	Run-Out	9	2000000
Badie/Tadros	11	SS-5-10	1	8	Run-Out	5	2500000
Mundie[3]	1	S-0.875-22-A	2	4	Type B/C	22	325557
Mundie	2	S-0.875-22-B	2	4	Type B/C	22	80346
Mundie	3	S-0.875-22-C	2	4	Type B/C	22	245121
Mundie	4	S-0.875-22-D	2	4	Type B/C	22	91598
Mundie	5	S-0.875-18-A	2	4	Type B/C	18	1586515
Mundie	6	S-0.875-18-B	2	4	Type B/C	18	2654243
Mundie	7	S-0.875-18-C	2	4	Type B/C	18	986718
Mundie	8	S-0.875-18-D	2	4	Type B/C	18	235326
Mundie	9	S-0.875-26-A	2	4	Type B/C	26	38295
Mundie	10	S-0.875-26-B	2	4	Type B/C	26	56507
Mundie	11	S-0.875-26-C	2	4	Type B/C	26	36094
Mundie	12	S-0.875-26-D	2	4	Type B/C	26	38101
Faust[4]	1	1	2	2	N.S.	16.1	566000
Faust	2	2	2	2	N.S.	16.1	522600
Faust	3	3	2	2	N.S.	16.8	720000
Faust	4	4	2	2	N.S.	20.57	83700
Faust	5	5	2	2	N.S.	20.94	103600
Faust	6	6	2	2	N.S.	21.32	96500
Faust	7	7	2	2	N.S.	24.31	60400
Faust	8	8	2	2	N.S.	15.71	550000
Faust	9	9	2	2	N.S.	14.97	907000
Faust	10	10	2	2	N.S.	14.97	913000
Faust	11	11	2	2	N.S.	23.57	39140
Provines/Ocel[5]	1	1F1	F.S.[6]	N.A.		20	175000
Provines/Ocel	2	2F1	F.S.	N.A.		20	174000
Provines/Ocel	3	3F2	F.S.	N.A.		20	51000
Provines/Ocel	4	4F1	F.S.	N.A.		20	91000
Provines/Ocel	5	2F2	F.S.	N.A.		16	260000
Provines/Ocel	6	3F1	F.S.	N.A.		16	747000
Provines/Ocel	7	4F2	F.S.	N.A.		16	680000

[1] Feldman, et al. (2011) [11]
[2] Badie, et al. (2002) [8]
[3] Mundie, D.L. (2011) [24]
[4] Faust, et al.(2000) [25]
[5] Provines, J., and Ocel, J.M. (2014) [26]
[6] Full-scale beam test

Appendix B. Material Test Data

B1. Concrete Cylinder Fabrication and Testing

Concrete compressive strength was determined for the slab of each push-out specimen using cylinder compression tests. Approximately 12 concrete cylinders were created and tested from each concrete batch (four specimen slabs) following procedures outlined in the ASTM specifications [27,28]. Because concrete strength can change over time, compressive testing of the concrete cylinders coincided with beginning of each fatigue test. Figure B- 1 shows the test setup used to determine concrete compressive strength, consisting of a Forney concrete compression machine capable of applying 400 kips of axial force. Also shown in Figure B- 1 is the sample concrete cylinder geometry. Note that while the push-out specimens contain two concrete slabs, created from two separate concrete batches, the material strengths provided in Table 1 of Section 2 represent the average concrete strength from both slabs.
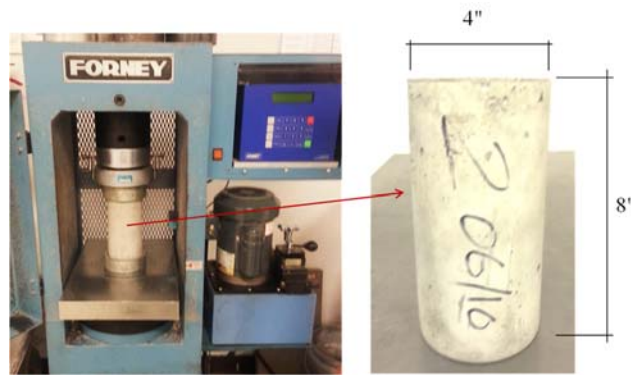
Figure B- 1. Concrete testing machine and cylinder dimensions

Table B-1 shows the age and strength of each individual concrete sample. In Table B-1 the number of cylinders available for material testing slightly varies between push-out specimens due to the amount of remaining concrete following casting.

Table B- 1. Concrete compression test data for push-out specimen slabs

	Concrete Compressive Strength, f'_c, MPa					
	1	2	3	4	5	6
Slab 1	42.0	47.3	40.2	54.2	46.8	58.4
	38.4	46.8	40.7	56.6	40.7	55.4
	--	47.2	--	61.4	--	51.9
	--	43.8	--	--	--	--
	--	47.7	--	--	--	--
	--	43.3	--	--	--	--
Slab 2	45.4	50.2	46.9	58.4	45.7	57.3
	37.6	49.7	48.9	56.8	--	58.2
	--	48.2	--	58.3	--	57.0
	--	48.2	--	--	--	--
	--	54.3	--	--	--	--
	--	50.9	--	--	--	--
Average f'_c, MPa	40.9	48.1	44.2	57.6	44.4	56.4
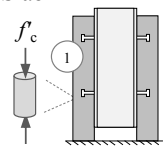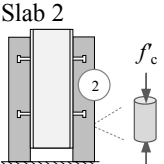
Appendix C. Verification of Negligible Inertial Effects under High Frequency Loading

To ensure appropriate applied stress ranges, all specimen loads applied in this study are determined by a controlled loop process driven by local load cell measurements (i.e. load controlled testing). Given that the load cell measurements are taken by a device mounted to the moving loading ram, at higher loading frequencies the possibility exists for inertial forces to influence load measurements and therefore the applied specimen loads.

To verify negligible inertial effects at higher frequency loadings and ensure consistency in the applied load across loading rates, the local slab slip response of the push-out specimens are compared under pseudo-static loading frequencies (1Hz) and high frequency loadings (20Hz). All slip measurements are taken from LVDTs locally mounted to the specimens. Figure C-1 shows the resulting slip versus time at 1Hz, 10Hz, and 20Hz loading frequencies for Specimen 5. From Figure C-1, peak displacement measurements remain similar across all loading rates. Assuming that the specimen stiffness remained relatively constant within 1,000 loading cycles, these similar slip readings indicate that the loads applied to the specimens are not influenced by inertial effects from the load cell movement at high frequencies.
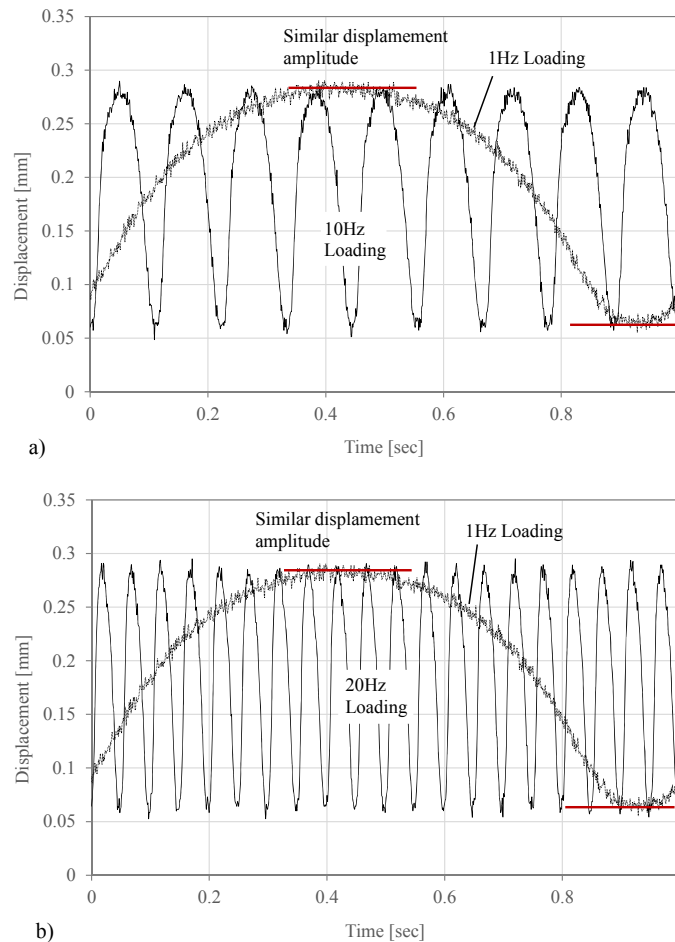
Figure C-1. Comparison of slab slip measurements for Specimen 5 during high frequency dynamic loading. Comparisons presented represent (a) 1Hz and 10Hz loading rates, and (b) 1Hz and 20Hz loading rates

Appendix D. Additional Slip and Separation Measurements

Slip and separation provide an indication of stud fatigue damage during testing. Figure D-1 provides the slip and separation data for Specimens 1, 3, 4, 5, and 6. Note that LVDT data for Specimen 2 is not provided as it was lost from the acquisition device during a power outage prior to test completion.

(a)   (b)
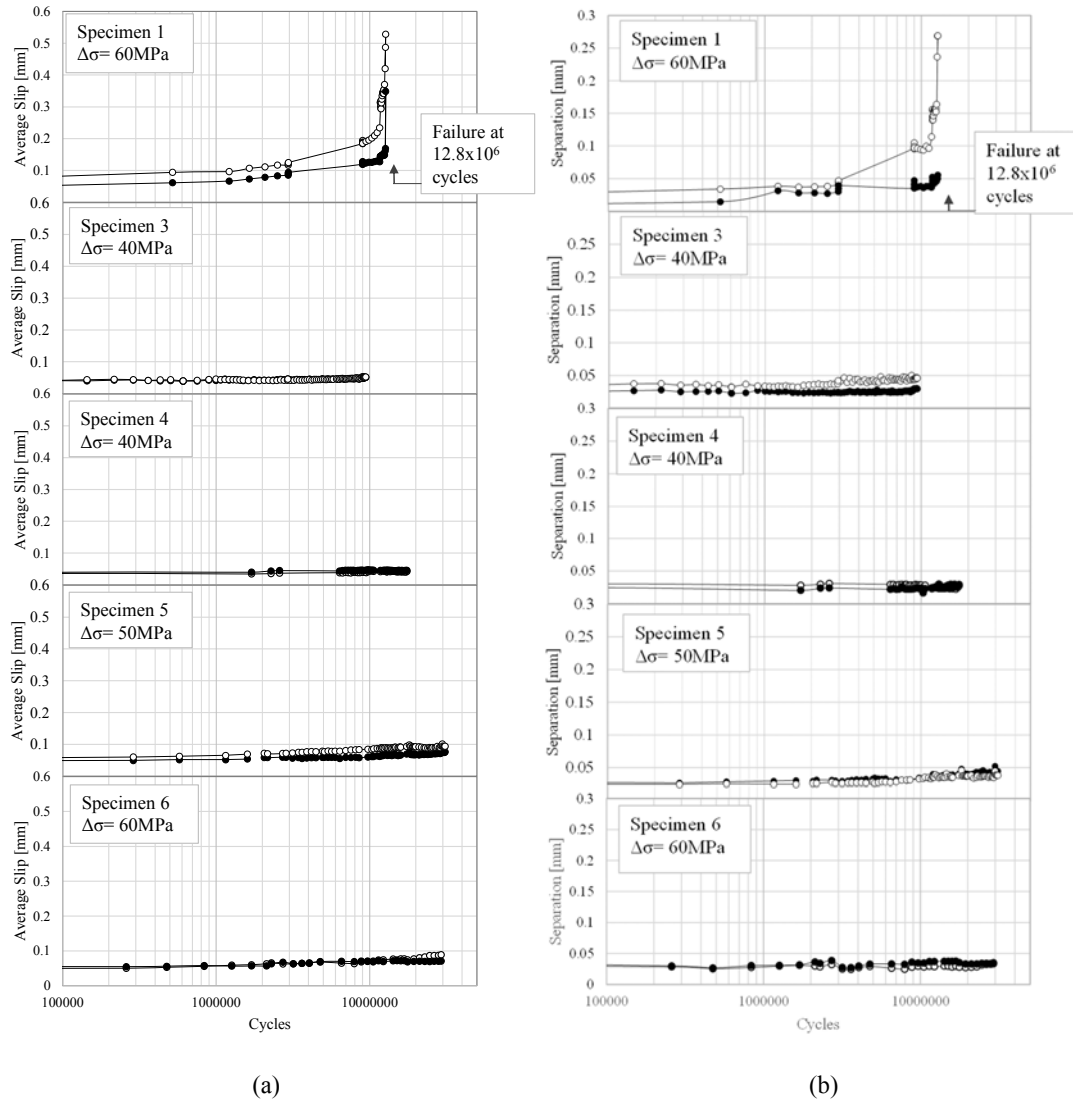
Figure D-1. (a) Slip and (b) separation data from external LVDT measurements